LA-UR-18-24035 (Accepted Manuscript)

# Nanochannel structures in W enhance radiation tolerance

Qin, Wenjing
Ren, Feng
Doerner, Russell P.
Wei, Guo
Lv, Yawei
Chang, Sheng
Tang, Ming
Deng, Huiqiu
Jiang, Changzhong
Wang, Yongqiang



**To be published in:** Acta Materialia

**DOI to publisher's version:** 10.1016/j.actamat.2018.04.048

**Permalink to record:** http://permalink.lanl.gov/object/view?what=info:lanl-repo/lareport/LA-UR-18-24035

# Accepted Manuscript

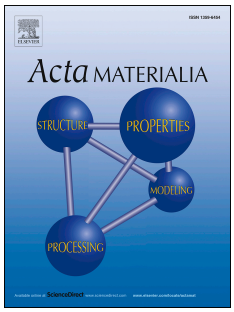


Nanochannel structures in W enhance radiation tolerance

Wenjing Qin, Feng Ren, Russell P. Doerner, Guo Wei, Yawei Lv, Sheng Chang, Ming Tang, Huiqiu Deng, Changzhong Jiang, Yongqiang Wang

PII: S1359-6454(18)30325-2

DOI: 10.1016/j.actamat.2018.04.048

Reference: AM 14536

To appear in: *Acta Materialia*

Received Date: 30 December 2017

Revised Date: 2 April 2018

Accepted Date: 19 April 2018

Please cite this article as: W. Qin, F. Ren, R.P. Doerner, G. Wei, Y. Lv, S. Chang, M. Tang, H. Deng, C. Jiang, Y. Wang, Nanochannel structures in W enhance radiation tolerance, *Acta Materialia* (2018), doi: 10.1016/j.actamat.2018.04.048.

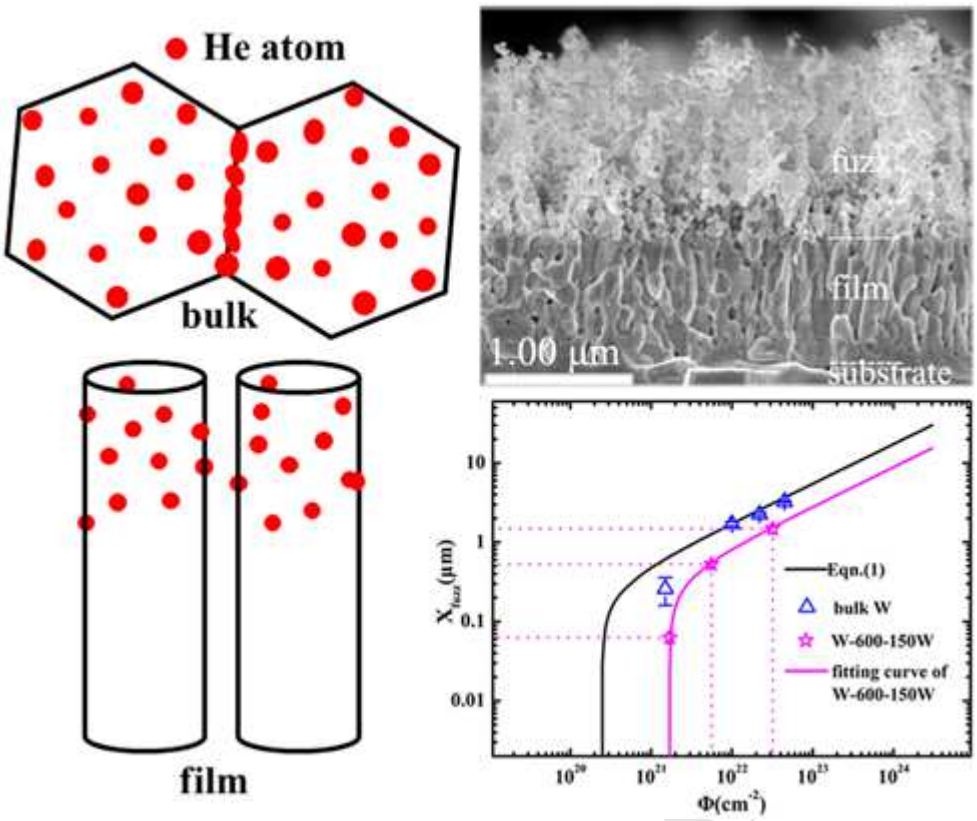

# Nanochannel structures in W enhance radiation tolerance

Wenjing Qin [a], Feng Ren [a]*, Russell P. Doerner [b], Guo Wei [a], Yawei Lv [a], Sheng Chang [a], Ming Tang [c], Huiqiu Deng [d], Changzhong Jiang [a], Yongqiang Wang [c]*

[a] School of Physics and Technology, Center for Ion Beam Application and Center for Electron Microscopy, Wuhan University, Wuhan 430072, China.

[b] Center for Energy Research, University of California at San Diego, La Jolla, California 92093, USA.

[c] Materials Science and Technology Division, Los Alamos National Laboratory, Los Alamos, New Mexico 87545, USA.

[d] Department of Applied Physics, School of Physics and Electronics, Hunan University, Changsha 410082, China

*e-mail: fren@whu.edu.cn +86 27 68752567 and yqwang@lanl.gov (505)665-1596

**Abstract**

Developing high performance plasma facing materials (PFMs) is one of the greatest challenges for fusion reactors, because PFMs face unprecedented harsh environments including high flux plasma exposure, fast neutron irradiation and large transmutation gas. Tungsten (W) is considered as one of the most promising PFMs. Rapid accumulation of helium (He) atoms in such environments can lead to the He bubbles nucleation and even the formation of nano- to micro-scale “fuzz” on W surface, which greatly degrade the properties of W itself. The possible ejection of large W particulates into the core plasma can cause plasma instabilities. Here, we present a new strategy to address the root causes of bubble nucleation and “fuzz” formation by concurrently releasing He outside of W matrix through the nano-engineered channel structure (nanochannels). Comparing to ordinary bulk W, nanochannel W films with high surface-to-volume ratios are found to not only delay the growth of He bubbles, but also suppress the

formation of “fuzz” (less than a half of the “fuzz” thickness formation in bulk W). Molecular dynamic (MD) simulation results elucidate that low vacancy formation energy and high He binding energy in the nanochannel surface effectively help He release and affect He clusters distribution in W during He ion irradiation.

**Keywords:** tungsten; nanochannel formation; bubble; “fuzz”; simulation

## 1. Introduction

Plasma facing materials (PFM) for fusion reactors suffer unprecedentedly harsh environments due to high fluxes of plasma particle collisions/erosions (He, H, D, T with energies of 10-$10^4$ eV and fluxes of $10^{18\text{-}20}$ ions/cm$^2$s), and 14.1 MeV neutron irradiations [1]. Finding a suitable PFM is one of the greatest challenges for fusion energy research. Tungsten (W) is a promising PFM (such as divertor) due to its desirable physical and chemical properties (high melting point, good thermal conductivity, low sputtering coefficient, low tritium retention rate and good optical reflectivity etc.). However, using W as a PFM also introduces other unique challenges. In fusion reactors, fast neutron irradiations produce much greater amount of transmuted He atoms than in fission reactors. These He atoms quickly precipitate into He bubbles, resulting in embrittlement and hardening problems of fusion reactor materials [2, 3]. Furthermore, under high flux He plasma exposure, high concentration of He atoms in W eventually leads to the formation of “fuzz” microstructure [4] at elevated temperatures, which has become one of the most serious issues for plasma facing W owing to significant degradations in its surface stability, thermal conductivity, optical reflectivity etc. Once the “fuzz” is peeled off, which will greatly affect the core plasma stabilities [5]. Therefore, understanding the interaction between He atoms and W plays an important role in the development of excellent performance W materials as PFM.

Although many previous studies revealed that grain boundaries [6] and interfaces [7, 8] can act as effective “sinks” to trap defects and store He bubbles, their bubble storing capabilities are limited, and the He embrittlement in grain boundaries and interfaces will inevitably form cracks when high concentration of He atoms are gradually built up. Since the root cause of the He bubble nucleation and its effect on the microstructure (e.g. “fuzz” formation) and properties (e.g. embrittlement) is the very low solubility of He atoms in W, timely releasing or outgassing He during the He bombardment should suppress rapid He built-up in the PFM and thus delay or slow “fuzz” formation and growth.

In this article, we present a new strategy by introducing a nanochannel incorporated microstructure to help address the root causes for both He bubbles and “fuzz” formation challenges faced by plasma facing W in fusion reactors. Experiments and theoretical simulations show that nanochannel W films are successfully produced through physical vapor deposition and exhibit to facilitate “self-healing” by releasing or outgassing He atoms to effectively retard the growth of He bubbles and suppress the formation and growth of “fuzz” as compared to those of bulk W.

## 2. Experimental

### 2.1. Materials preparation

Nanochannel W films with different nanochannel densities were deposited on silicon (100) substrates using ultrahigh vacuum DC magnetron sputtering deposition (ULVAC, ACS-4000-C4). In order to obtain films with different nanochannel densities, the three kinds of nanochannel W films were prepared under different temperatures and powers: room temperature (RT) and 150 Watt, 600 ºC and 150 Watt, 600 ºC and 50 Watt, and these three different samples were named as W-RT-150W, W-600-150W and W-600-50W, respectively. Thicknesses of the three nanochannel

W films were approximately 1 micrometer. In order to compare the properties of the nanochannel W films with bulk materials, polycrystalline bulk W specimens (99.95 wt.% purity, ATTL Advanced Materials Co., Ltd.) with dimensions of 10 mm×10 mm×0.4 mm were also prepared. The bulk W specimens was mechanically polished to a mirror finish and then annealed at 1200 K for 2 h in vacuum with background pressure of $2.5\times10^{-4}$ Pa [9]. The surface morphology and grain orientation of bulk W are shown in Supplementary Fig. S1. In addition, considering the requirements of the following He plasma exposure experiment, the nanochannel W films were directly deposited on mechanically polished W molds and detailed description and discussion on nanochannel W films deposited on different substrates were presented in the Fig. S2-S3.

**2.2. High energy $He^+$ ion irradiation**

To quantitatively study the He distribution in nanochannel W films, we first used a well-controlled ion implantation process to investigate the He retention and bubble formation behaviors. The nanochannel W films and bulk W were bombarded with a 40 keV $He^+$ ion beam to fluences up to $10^{18}$ ions/cm$^2$ under RT with a flux of ~$1.5\times10^{13}$ ions/cm$^2$s on a 200 keV ion implanter (LC22-100-01). The displacement per atom (dpa) and He concentration were calculated by SRIM-2013 [10] in "Quick Kinchin-Pease" mode. The threshold displacement energy of W atoms used was 90 eV [11]. The simulation results are shown in Fig. S4. According to the simulation results, the peak damage is approximately 1.26 dpa (displacement per atom) at the depth of 60 nm and the peak He concentration is about 10.8 at.% at the depth of 108 nm under the fluence of $1\times10^{17}$ ions/cm$^2$.

**2.3. Low energy He plasma exposure**

To investigate the influence of nanochannel structure on the "fuzz" formation caused by the rapid accumulation of He bubbles, the He plasma exposure was done on the linear divertor

plasma simulator PISCES-A at University of California in San Diego. The He ion flux on samples was ~5.0-6.5×$10^{18}$ ions/$cm^2$s. According to the reports of previous studies, the "fuzz" formation is closely related with the incident ion energy and surface temperature. When the incident ion energy is higher than 20 eV and the surface temperature is in the range of 1000-2000 K, the "fuzz" is easy to form on the surface of W. Because when the incident ion energy below the 20 eV, the efficiency of the nanostructure formation is relatively low and only pinholes are formed on the surface. When the temperature is below 900 K, low mobility of He and vacancies are not sufficient to form large bubbles and fail to form "fuzz", while the temperature higher than 2000 K makes the "fuzz" disappeared [12, 13]. In addition, taking into account the sputtering yield of the W "fuzz" [14], in this experiment, the bias was set to -60 V, thus giving an incident ion energy of ~50 eV. The samples were heated by plasma and the irradiation time started counting from the temperature up to ~1073 K, at the same time cooling was increased until the temperature kept at ~1140 K. The irradiation time was 300, 1100 and 5000 s, respectively.

**2.4. Simulation method**

To better explore the influence of nanochannel microstructure on He release, and further explain the reason that the nanochannel W film can effectively inhibit the growth of "fuzz", molecular dynamics (MD) simulations were performed to understand He behavior and their evolution in the nanochannel W films and bulk W structures by using a Large-scale Atomic/Molecular Massively Parallel Simulator (LAMMPS) [15] code. The relevant interatomic potentials among W-He was developed by Juslin and Wirth [16]. Based on the structures of the prepared nanochannel W films, a corresponding simulation model of W columnar crystal within the film along (100) surface (Model I) was obtained (see Fig. S5). The columnar crystal diameter was 20$a$ and the size of simulation box was set as $24a \times 24a \times 35a$, where the lattice parameter $a$

was 3.1652 Å at 300 K, 3.189 Å at 1140 K, respectively. Two-dimensional periodic boundary conditions were used in the *x* and *y* directions, thus the distance between two adjacent columnar crystal was 4*a*. The top of *z* direction was a free surface and along (100) plane, in which two layers of atoms were fixed at the bottom to avoid the net drift of atoms [17]. Accordingly, a nanochannel W film but the W columnar crystal within the film have no (100) surface was also simulated for comparison (Model II), which means that the W columnar crystal is one infinite W nanowire with periodic boundary conditions. In addition, a bulk W specimen with one (100) surface was also simulated with the same bottom area and height of nanochannel W film, where two-dimensional periodic boundary conditions are used perpendicular to the surface (Model III). To simulate the He plasma exposure on W film, the same incident energy 50 eV was chosen. The He ion flux was about $2.0\times10^{27}$ $m^{-2}s^{-1}$. Two different temperatures of 300 and 1140 K were set to analyze the influence of temperature on the He release and the formation of He clusters. The implanted total He number was 1000. Under each simulation condition, 10 independent cascade simulations were performed to reduce the statistical error.

**2.5. Characterization method**

The surface and cross-sectional morphology of samples were characterized by scanning electron microscope (SEM, Hitachi S-4800). Cross-sectional transmission electron microscopy (XTEM) images of the irradiated samples were performed using a JEOL JEM-2010 (HT) (TEM) operating at 200 kV. The TEM samples were prepared by traditional processes including hand grinding, dimple and ion milling, in which the ion milling was performed by Precision Ion Polishing System (Gatan 691) with $Ar^+$ ion energies of 2.5-4.5 keV and ion beam angles of 3º ~ 4.5º to reduce the damage caused by ions. The crystalline structure of the pristine samples was identified by grazing incidence X-ray diffraction (GIXRD, a Bruker AXS D8 Advanced X-ray

diffractometer with Cu $K\alpha$ radiation) with tilting angle of 0.5°. The densities of the nanochannel W films were measured by Rutherford backscattering spectrometry (RBS). The retained He concentrations in the irradiated samples to the different fluences were measured by elastic recoil detection (ERD). The ERD was performed using a 12 MeV $^{12}C^{3+}$ analyzing beam oriented 75.5° to the samples normal. The GIXRD, RBS and ERD measurements were carried out at Ion Beam Materials Laboratory in Los Alamos National Laboratory.

## 3. Results and discussion

### 3.1. The microstructure of nanochannel W films

While porosity needs to be avoided or minimized during the film growth or materials synthesis in most applications since it contributes to decrease structural properties, here we use it to our advantage in effectively managing He effects in W where the PFM is mainly used as a functional barrier rather than a structural material. Fig. 1a-1c show XTEM images of the three nanochannel W films, where the inserts show the surface and cross-sectional SEM images of the corresponding films. Nanochannels are clearly formed between columnar crystals during the film deposition. Fig. 1d shows GIXRD patterns from these nanochannel W films. The nanochannel W-RT-150W film exhibits a metastable β-phase with A-15 crystalline structure, the nanochannel W-600-150W and W-600-50W films are in a stable α-phase with body centered cubic (bcc) structure as a result of heating effects and low oxygen impurity concentrations [18]. Using the actual film thickness (~1 μm) measured by XTEM, densities of the as-deposited nanochannel W-RT-150W, W-600-150W and W-600-50W films determining by RBS are 15.86, 17.46 and 18.07 g/cm$^3$, respectively. As expected, these values are lower than that of the bulk W (19.3 g/cm$^3$) due to the formation of nanochannels inside the films. Statistical analyses from SEM and XTEM images find that the average columnar sizes in the nanochannel W-RT-150W, W-600-150W and

W-600-50W films are approximately 64.2, 92.9 and 168.4 nm (Fig. S6), respectively, indicating that the nanochannel W-600-50W film contains the fewest number of nanochannels, which is consistent with its highest density from the RBS measurement.

Due to high surface energy, low diffusion rate of W and the atomic shadowing effects, the nanochannel W films grow to be columnar crystal structure under the condition of magnetron sputtering deposition [19]. Because the diffusion ability rate of sputtering atoms is a main factor to determine microstructure and columnar size of thin film, the nanochannel densities of W films can be tailored by controlling substrate temperatures and sputtering powers during deposition process. At low substrate temperature, the film is easily formed by small and elongated grains and gradually grow into a columnar crystalline structure with porous morphology. With higher substrate temperature, a denser columnar crystalline structure is produced due to faster diffusion of sputtering atoms. Meanwhile, under the same substrate temperature, low deposition rate under low sputtering power results in the increase of columnar crystal size comparing to that deposited under high sputtering power [20].

### 3.2. Helium bubbles distribution after 40 keV $He^+$ ions irradiation

Our TEM measurements observed no visible He bubbles in all samples even after the high fluence irradiation of $1\times10^{17}$ ions/cm$^2$. Furthermore, only small bubbles are observed under the next higher fluence of $3\times10^{17}$ ions/cm$^2$ (corresponding to a peak He concentration of ~32.4 at.%). Fig. S7 shows the XTEM micrographs of these 40 keV $He^+$ ions irradiated nanochannel W-RT-150W, W-600-150W, W-600-50W films and bulk W to the fluence of $3\times10^{17}$ ions/cm$^2$, where the Gaussian-distributed small bubbles along the depth are observed in the nanochannel W films and bulk W, consistent with the simulated distribution of He atoms by SRIM-2013. These results are not unexpected considering the fact that the formation energy of one He atom in the

tetrahedral interstitial site (TIS) of W bulk (6.14 eV [21]) is much larger than that in other metals--e.g. Fe (4.61 eV [21]), Cu (4.00 eV [21]), etc., implying the formation of He clusters or bubbles in W requires a super high He concentration.

To further study the influence of nanochannel structures on managing bubbles, the nanochannel W films and bulk W were irradiated to higher fluences. When the fluence is increased to $5\times10^{17}$ ions/cm$^2$ (Fig. 2$a_1$-2$d_1$), He bubbles in the irradiated samples continues to grow larger by absorbing new incoming He atoms or dissociative vacancies. It should be noted that while no cracks are found at this high fluence in any of the nanochannel W films (Fig. 2$a_1$-2$c_1$), ~5 nm-wide cracks are already observed in the bulk W (Fig. 2$d_1$) at the projected depth of the peak He concentration due to the aggregation of He atoms. When the fluence is further increased to $1\times10^{18}$ ions/cm$^2$, the width of cracks in bulk W expand to ~11 nm. Surprisingly, none of the nanochannel W films have shown any cracks, although the nanochannel W-600-50W film starts to show coalescence of some bubbles into bubble lines (Fig. 2$a_2$-2$c_2$). This is remarkable considering that the estimated peak He concentration at the projected depth is approaching ~100 at.% at such a super high fluence. The results of these cracks imply that the partial of incident He atoms in the nanochannel W films might have been released along the nanochannels rather than accumulated into large pressurized bubbles.

At low temperature, the radiation-induced vacancy cannot migrate, the implanted He atoms are easily trapped by vacancies to form clusters. With the increase of He atoms number, the He clusters gradually nucleate and grow into He bubbles [22]. The average bubble sizes and areal densities in the samples irradiated to different fluences measured from the XTEM images are shown in Fig. 3. To reduce the statistical error as much as possible, all TEM images used for statistics were kept at the same defocus value. On the whole, the average He bubble sizes

increase with the increase of fluence, while the change trend of bubble areal densities is just opposite. In the bulk W, the average bubble sizes are slightly larger than that in the nanochannel W films, and the bubble areal densities are much larger than that in the nanochannel W films at the same fluence. For the nanochannel W films, the average bubble sizes increase with increasing nanochannel density, while the bubble areal densities changes in opposite. The changes of average bubble sizes and areal densities indicate that the He bubbles concentrations in the W films decrease with increasing the nanochannel densities and are much lower than those found in the bulk W. These results further demonstrate nanochannel W films have the potential to effectively manage He bubbles.

To confirm the XTEM results above and further quantitatively measure the effectiveness of He release capacity by nanochannels in the W films, ERD analysis was used to measure He atoms in the irradiated samples. To simplify the comparative analysis, the irradiated bulk W to the fluence of $3\times10^{17}$ ions/cm$^2$ was used as a reference sample in which no He atoms are assumed to be escaped from the sample during the irradiation. The He concentrations of all the other irradiated samples were then calculated in relating to the reference sample and the results were summarized in Table 1. The ratios of He retention in the nanochannel W-RT-150W, W-600-150W, W-600-50W films and bulk W at the fluence of $3\times10^{17}$ ions/cm$^2$ are 88.3%, 97.7%, 99.3% and 100%, respectively. When the fluence is increased to $5\times10^{17}$ ions/cm$^2$, the ratios decrease to 70.4%, 89.8%, 95.6% and 90.8%, respectively. For the highest fluence of $1\times10^{18}$ ions/cm$^2$, the ratios further decrease to only 36.3%, 53.8%, 49.8% and 52.3%, respectively. According to ERD tests, only a small amount of He release is observed in the nanochannel W films irradiated to $3\times10^{17}$ ions/cm$^2$. While the amount of He release increases noticeably when the fluence increases to $5\times10^{17}$ ions/cm$^2$, and then substantially when the fluence further increases to $1\times10^{18}$ ions/cm$^2$. It

is not anticipated, the He retention in the nanochannel W-600-150W film is slightly higher than that in the nanochannel W-600-50W film at the fluence of $1\times10^{18}$ ions/cm$^2$. The reason may be that some in-line bubbles in the nanochannel W-600-50W film may be extended into nanochannels to facilitate the migration of He atoms out of the film [23]. It should be noted that a large amount of He is also released from the bulk W at the high fluences due to the escape of He from large cracks. However, such He release is uncontrollable, the formation of cracks greatly decreases structural stability and thus shorten service lifetime of bulk W. In short, the ERD measurements clearly confirm that the nanochannel structure can effectively releases He atoms out of the films, reducing He concentration, remaining its structure and preventing the formation of larger bubbles and cracks.

These experimental observations lead us to hypothesize that the W films containing abundant interspersed nanochannels with rich free unsaturated surfaces act as “sinks” to effectively trap and release He atoms out of the films along the nanochannels during the He irradiation as depicted in Fig. 2e. In other word, these nanochannel W films have higher radiation tolerance with a “self-healing” capability, particularly in effectively managing He bubbles compared with the bulk W.

### 3.3. The formation of “fuzz” under 50 eV He plasma exposure

Based on the performance data from 40 keV $He^+$ ions irradiation experiments above, although the nanochannel W-RT-150W film has the best performance in managing He bubbles, β-phase W is metastable with relatively poor electrical conductivity (thus poor thermal conductivity) compared to that of stable α-phase W [24], therefore, the most promising nanochannel W-600-150W was chosen for the linear plasma exposure test. Fig. 4a-4c display SEM images of the nanochannel W-600-150W film exposed to 50 eV He plasma at 1140 K to the fluences of

$1.7\times10^{21}$, $5.6\times10^{21}$, and $3.2\times10^{22}$ ions/cm$^2$, respectively. At the lowest fluence ($1.7\times10^{21}$ ions/cm$^2$), many pinholes are observed on the film surface. At the higher fluence of $5.6\times10^{21}$ ions/cm$^2$, nano-structural "fuzz" are formed. At the highest fluence of $3.2\times10^{22}$ ions/cm$^2$, the "fuzz" diameter becomes smaller while its length elongates. The corresponding thicknesses of "fuzz" layers measured from the cross-sectional SEM images are plotted in Fig. 4d. The thickness of the "fuzz" layer is approximately 63 nm at the fluence of $1.7\times10^{21}$ ions/cm$^2$, and quickly grows to ~529 nm and ~1.5 μm as the fluence increases to $5.6\times10^{21}$ and $3.2\times10^{22}$ ions/cm$^2$, respectively. Surprisingly, both the surface "fuzz" structures and remaining nanochannel W films do not be peeled off from the W substrate in such harsh environment, the remaining film thicknesses are plotted against the He fluence in Fig. 4e. Clearly, the whole film of ~1 μm thick is only reduced by ~72 nm under the highest fluence of $3.2\times10^{22}$ ions/cm$^2$ (approximately 5000 s exposure). It is important to note that the typical columnar or nanochannel feature below the "fuzz" layer is largely preserved even after such a high temperature and high He flux exposure, indicating a good durability of these nanochannel W structures.

In order to evaluate the "fuzz" structure formation in the nanochannel W films, "fuzz" thickness values of typical bulk W [25] (Table S1) under similar experimental conditions are used as a contrast. These reference values of bulk W are plotted in Fig. 4d, which shows that the "fuzz" thickness of bulk W is more than the double of the nanochannel W-600-150W film under similar exposure conditions. More quantitatively, since the incident ion energy ~ 50 eV is below the sputter yield [26], thus, "fuzz" thickness ($x$) depends on He fluence ($\Phi$) and is described by the Equation [25]:

$$x(\Phi) = (C(\Phi - \Phi_0))^{1/2} \quad (1)$$

where $C=2D/\Gamma$ with $\Gamma$ is ion flux and $D$ is effective diffusion coefficient ($D$ actually represents

the growth rate of "fuzz" [27]). The previous He plasma experiment on bulk W [25] shows that the incubation fluence ($\Phi_0$) for the formation of any observable "fuzz" on bulk W is approximately $2.5\times10^{20}$ ions/cm$^2$. However, as shown in Fig. 4a, the incubation fluence of ~$1.7\times10^{21}$ ions/cm$^2$ as determined for the nanochannel W-600-150W film is one order higher than that of bulk W, implying that the nanochannel W film can effectively suppress the formation of "fuzz" structure and is more resistant to plasma irradiation than the bulk W. Furthermore, the effective diffusion coefficient ($D$=$7.54\times10^{-12}$ cm$^2$/s) in the bulk W at 1140 K is calculated based on the values of $D_{1120\ K}$ and $D_{1320\ K}$ from the Ref. [27]. Applying the ion flux of ~$5\times10^{18}$ ions/cm$^2$s used in this experiment, the black curve predicted from Eqn. (1) is included in Fig. 4d. By fitting experimental values of "fuzz" thickness of the nanochannel W-600-150W film, a magenta curve is generated, which is also plotted in Fig. 4d. Subsequently, the effective diffusion coefficient for the nanochannel W film is obtained as ($D$=$1.95\times10^{-12}$ cm$^2$/s) according to Eqn. (1), which is significantly lower than that of the bulk W ($D$=$7.54\times10^{-12}$ cm$^2$/s). It should be noted that $D$ describes the observed growth rate of "fuzz", meaning that there is much lower growth rate of "fuzz" in the nanochannel W films than in the bulk W.

During the low-energy He plasma exposure, no vacancies are formed in the knock-on process, He atoms can easily form clusters by self-trapping. Because small He clusters can also diffuse at the high temperature, it is easy to form large He clusters below the surface. With the growth of He clusters, the pressurized He clusters can punch out the self-interstitial W atoms and occupy the vacancies to form helium-vacancy clusters and gradually form He bubbles [5, 28]. Many experimental and simulation researches have focused on the formation and growth mechanism of the "fuzz", there are three mainly processes can be concluded: i. Due to the accumulation of many He bubbles below the surface, the lattice of W atoms becomes strained, gradually the W

atoms are shifted, thus causing the surface lifting. ii. As the fluence increases, pressures in the He bubbles become larger and larger. When the pressure of He bubbles exceed a certain threshold, He bubbles will burst and form pinholes, dips or protrusions on the surface. iii. As the fluence continues to increase, incident helium atoms are injected into these convex, flat or concave surfaces. Ito et al. [29] found, by Molecular dynamic and Monte Carlo simulations, that more He bubbles were accumulated and burst under the concave surface, resulting in irregular structural enhancement, because incident He atoms were more difficult to escape from the concave surface compared to the convex and flat surfaces. With the growth and accumulation of He bubbles, the lifting and burst processes will occur again, leading to the formation and continued growth of the "fuzz" structure. According to above processes, it can be concluded that He bubbles growth and loop-punching are the root reasons for the formation and growth of "fuzz" structure, and the He concentration is the most critical factor [5, 13, 29-31]. Furthermore, Fiflis et al. [31] proved by experiments that continued growth of the "fuzz" structure was still from bottom up even when the "fuzz" had been formed. It can be inferred that under the same irradiation fluence, due to the great release of incoming He through the additional introduced nanochannel surface, the He concentration in the nanochannel W films is much lower than that in the bulk W, meanwhile, the lattice stress due to the growth of He bubbles can also be reduced by the nanochannels. Therefore, the incubation fluence that is required to form "fuzz" structure on nanochannel W film increases. On the other hand, the number of highly pressurized He bubbles in the nanochannel W films are lower than that observed in the bulk counterpart, resulting in a comparatively slower growth rate of "fuzz" in the nanochannel W films. Under such high flux He plasma exposure and high temperature conditions, the surface of W material will be seriously eroded when the "fuzz" structure is formed. However, only ~72 nm thickness nanochannel W

films were transferred to “fuzz” structure during such long time (~5000 s) irradiation, which also proves that even under low-energy He plasma exposure, the nanochannel W film can still maintain good structure. Therefore, in such a harsh environment, nanochannel structure can still inhibit the “fuzz” formation and delay the “fuzz” growth.

### 3.4. Simulation of He behavior and evolution

To obtain the statistics of He atoms and highlight the effect of nanochannel on the He release, three atomistic models for the W-He system have been used during our MD simulation. The fraction of He atoms at different temperature in the three models have been obtained, as shown in Fig. 5a. At 300 K, the fraction of He retained in the nanochannel W film (Model I) is 50.5%, while 61.4% He atoms is retained in film without surface (Model II); therefore, the large amount of He released from nanochannel surface can be confirmed. Compared the He retention in the nanochannel films with and without top surfaces irradiated at 1140 K, it is not difficult to see that the He released from nanochannels is significantly enhanced and much higher than those released from top surface. It indicates that nanochannels alone can potentially release He atoms, validating their function as an effective facilitator for He release. To further illustrate the fact that nanochannel W films have better ability than the bulk W in “sink” He atoms, the number of He retention in the bulk W (Model III) was also calculated and used for comparison. At 300 K, the fraction of He retained in the bulk W is 70.5%, which is about 20% higher than that in the film. With the temperature increasing, the retention of He in the bulk W (47%) is approximately two times higher than that in the film (20.6%). From the present simulation results, it can be seen that He concentration in the nanochannel W film is smaller than that in the bulk W because the nanochannels can effectively help He release out of the film, which is also well verified the above experimental results.

It is well known that He clusters can form easily during the diffusion processes. To understand the influence of nanochannel structures on the evolution of He atoms more detailed, the size distribution of $He_n$ cluster after being implanted with 1000 He atoms was obtained and shown in Fig. 5b. It can be found that, at 300 K, many large He clusters are inclined to be formed in the bulk W, and the number of small He clusters (n<7) in the bulk W is less than those in the nanochannel W film. As the high temperature can effectively promote the diffusion of interstitial He atoms and He clusters, the increase of He release significantly decreases in the total numbers of He clusters formed at 1140 K. Obviously, compared with the bulk W, no large He clusters (n>50) are found in the nanochannel W film because the He atoms in the film are effectively released out rather than forming many large clusters. More intuitive distributions of He clusters in the film and bulk are shown in Fig. S8. The formation of smaller He clusters in the film makes it impossible to punch out the interstitial W atoms, and thus the formation and growth of “fuzz” is delayed. Therefore, the simulation results indicate that the existence of the nanochannel structures can effectively increase the He release, reduce the He concentration and suppress the formation of large clusters in the film. Compared with the bulk W, the nanochannel W films can better delay the growth of He bubbles and inhibit the formation of “fuzz”.

The vacancy and vacancy cluster can effectively trap He atoms and greatly affect the distribution of He clusters or even He bubbles in host materials. The binding energy between He atoms will affect their clustering [32, 33]. The existence of nanochannels essentially increases the proportion of free surfaces in the film; therefore, to highlight the influence of surface on He behaviors in W, the formation energy of vacancy and the binding energy between different He atoms near the W surface have been analyzed in the following: the formation energy of vacancy can be expressed as [34, 35]:

$$E_{\mathrm{V}}^{\mathrm{f}} = E_{\mathrm{S,V}} - E_{\mathrm{S}} + E(\mathrm{W}) \quad (2)$$

where $E_{\mathrm{S,\,V}}$ is the total energy of the W surface with one vacancy at a certain depth, $E_{\mathrm{S}}$ is the total energy of the W surface without vacancies, $E$(W) is the energy of per W atom in the perfect bcc lattice. The simulation results are shown in Fig. 6a. Clearly, the vacancy formation energy near the surface is greatly reduced, suggesting large amounts of vacancies are easily formed near the nanochannel surface, which can trap much more incident He atoms, reducing the He numbers in the columnar crystals. Furthermore, since He atoms have closed-shell electronic structures, they prefer to assemble each other by self-trapping and form He clusters [36, 37], which also influence the distribution of He concentration. In order to explore the influence of surfaces on the He self-trapping, the binding energies of two He atoms at different depths from the surface are calculated. The relevant formula is as follows [37]:

$$E_{\mathrm{b}} = 2E_{\mathrm{S,\,He}} - E_{\mathrm{S,\,2He}} - E_{\mathrm{S}} \quad (3)$$

where $E_{\mathrm{S,\,He}}$, $E_{\mathrm{W,2He}}$ and $E_{\mathrm{S}}$ are the total energies of W surface with one He atom, two He atoms and without He atoms, respectively. As described in Refs. [37-39], the TIS is the most stable interstitial sites for He atoms in original W unit cell. The binding energy of two second nearest neighbor TIS He atoms at positions 1 and 3 in the bulk W (see Fig. 6b) is first calculated and the result is 0.861 eV, which is well consistent with the reported value of 0.86 eV in Ref. [16]. To simplify the calculation, two first nearest neighbor TIS He atoms at positions 1 and 2 are selected to calculate their binding energies in different depths from the surface, as seen in Fig. 6b. Obviously, the closer to the surface, the higher the binding energy between He and He atoms, indicating that more He atoms will accumulate near the surface. Thus, the existence of large proportion nanochannels in W film leads to lower vacancy formation energy and higher He binding energy, which will promote the accumulation of He atoms near the nanochannel surface.

These He atoms that accumulate near the surface will form He clusters or even He bubbles through vacancy trapping or self-trapping. According to the description of He release in Refs. [40-42], when the He concentration in clusters or bubbles reaches a certain critical value, He atoms can be released by cluster or bubble bursting. And the pinholes formed on the surface will also be healed by thermal evolution of the substrate. This result can also be verified from the results of ERD tests (Table 1), the proportion of He released at $1\times10^{18}$ $He^{+}$ ions/$cm^{2}$ (63.7%) is higher than that released at $5\times10^{17}$ $He^{+}$ ions/$cm^{2}$ (29.6%). More detailed simulations to explain the reason are still under exploring. Based on the above discussion, we can conclude that the He atoms in the nanochannel surface can be released quickly through the "self-healing" nanochannels, rather than accumulating at grain boundary like bulk W, which effectively reduces the He concentration in the nanochannel W film. In addition, the nanochannels can be treated as free surface with image force and can accelerate the migration of He atoms to the nanochannel surface [43], providing a possible mechanism for He releasing. Therefore, the nanochannel W films with a large number of free surfaces have a relative lower He concentration than bulk W in the same irradiation condition.

## 4. Conclusion

In summary, nanochannel W films were synthesized and studied as a promising potential PFM candidate for fusion energy applications. Compared with the bulk W, abundant free surfaces of nanochannel W films act as efficient "sinks", quickly trapping and releasing He atoms along the nanochannels, and, as a result, retarding He bubble formation and reducing "fuzz" thickness. Therefore, the nanochannel W films show a potential as PFM alternatives to bulk W in fusion energy research and development.

**Acknowledge**

We thank Prof. W. Y. Hu for their useful discussions. Prof. Ren thanks the Natural Science Foundation of China (11522543, 11475129, 51771073 and 51571153), the Fundamental Research Funds for the Central Universities (2042017kf0194) and the Natural Science Foundation of Hubei Province, China (2016CFA080) for financial support. Both Doerner and Wang thank the support by the University of California Office of President Research Fund under Award Number 12-LR-237801. Wang also acknowledges the support by a Los Alamos Laboratory Directed Research and Development Fund (LDRD-20160567ER) and by the Center for Integrated Nanotechnologies (CINT), a DOE nanoscience user facility jointly operated by Los Alamos and Sandia National Laboratories. The numerical calculations in this paper have been done on the supercomputing system in the Supercomputing Center of Wuhan University.

**References**

[1] J. Knaster, A. Moeslang, T. Muroga, Materials research for fusion, Nature Physics 12(5) (2016) 424-434.

[2] C. Linsmeier, B. Unterberg, J.W. Coenen, R.P. Doerner, H. Greuner, A. Kreter, J. Linke, H. Maier, Material testing facilities and programs for plasma-facing component testing, Nuclear Fusion 57(9) (2017) 092012.

[3] J. Ongena, R. Koch, R. Wolf, H. Zohm, Magnetic-confinement fusion, Nature Physics 12(5) (2016) 398-410.

[4] M. Patino, Y. Raitses, R. Wirz, Secondary electron emission from plasma-generated nanostructured tungsten fuzz, Applied Physics Letters 109(20) (2016) 201602.

[5] Y. Ueda, K. Schmid, M. Balden, J.W. Coenen, L. Th, A. Ito, A. Hasegawa, C. Hardie, M. Porton, M. Gilbert, Baseline high heat flux and plasma facing materials for fusion, Nuclear Fusion 57(9) (2017) 092006.

[6] O. El-Atwani, J.A. Hinks, G. Greaves, S. Gonderman, T. Qiu, M. Efe, J.P. Allain, In-situ TEM observation of the response of ultrafine- and nanocrystalline-grained tungsten to extreme irradiation environments, Scientific reports 4 (2014) 4716.

[7] L. Dong, H. Zhang, H. Amekura, F. Ren, A. Chettah, M. Hong, W. Qin, J. Tang, L. Hu, H. Wang, C. Jiang, Period-thickness dependent responses of Cu/W multilayered nanofilms to ions irradiation under different ion energies, Journal of Nuclear Materials 497 (2017) 117-127.

[8] H. Wang, F. Ren, J. Tang, W. Qin, L. Hu, L. Dong, B. Yang, G. Cai, C. Jiang, Enhanced radiation tolerance of YSZ/Al2O3 multilayered nanofilms with pre-existing nanovoids, Acta Materialia 144 (2018) 691-699.

[9] B. Tyburska, V.K. Alimov, O.V. Ogorodnikova, K. Schmid, K. Ertl, Deuterium retention in self-damaged tungsten, Journal of Nuclear Materials 395(1-3) (2009) 150-155.

[10] J.F. Ziegler, M.D. Ziegler, J.P. Biersack, SRIM – The stopping and range of ions in matter (2010), Nuclear Instruments and Methods in Physics Research Section B: Beam Interactions with Materials and Atoms 268(11) (2010) 1818-1823.

[11] O.V. Ogorodnikova, B. Tyburska, V.K. Alimov, K. Ertl, The influence of radiation damage on the plasma-induced deuterium retention in self-implanted tungsten, Journal of Nuclear Materials 415(1) (2011) S661-S666.

[12] S. Kajita, W. Sakaguchi, N. Ohno, N. Yoshida, T. Saeki, Formation process of tungsten nanostructure by the exposure to helium plasma under fusion relevant plasma conditions, Nuclear Fusion 49(9) (2009) 095005.

[13] M.J. Baldwin, R.P. Doerner, Formation of helium induced nanostructure ‘fuzz’ on various tungsten grades, Journal of Nuclear Materials 404(3) (2010) 165-173.

[14] D. Nishijima, M.J. Baldwin, R.P. Doerner, J.H. Yu, Sputtering properties of tungsten 'fuzzy' surfaces, Journal of Nuclear Materials 415(1) (2011) S96-S99.

[15] S. Plimpton, Fast Parallel Algorithms for Short-Range Molecular Dynamics, Journal of Computational Physics 117(1) (1995) 1-19.

[16] N. Juslin, B.D. Wirth, Interatomic potentials for simulation of He bubble formation in W, Journal of Nuclear Materials 432(1–3) (2013) 61-66.

[17] J.L. Wang, L.L Niu, X.L. Shu, Y. Zhang, Stick–slip behavior identified in helium cluster growth in the subsurface of tungsten: effects of cluster depth, Journal of Physics: Condensed Matter 27(39) (2015) 395001.

[18] F.T.N. Vüllers, R. Spolenak, Alpha- vs. beta-W nanocrystalline thin films: A comprehensive study of sputter parameters and resulting materials' properties, Thin Solid Films 577 (2015) 26-34.

[19] F. Ying, R.W. Smith, D.J. Srolovitz, The mechanism of texture formation during film growth: The roles of preferential sputtering and shadowing, Applied physics letters 69(20) (1996) 3007-3009.

[20] E. Alfonso, G. Cubillos, J. Olaya, Thin film growth through sputtering technique and its applications M. Andreeta (Ed.), Crystallization – Science and Technology, InTech, Rijeka (2012), pp. 397-432.

[21] J.L. Cao, W.T. Geng, Migration of helium-pair in metals, Journal of Nuclear Materials 478 (2016) 13-25.

[22] H. Zhang, F. Ren, Y. Wang, M. Hong, X. Xiao, W. Qin, C. Jiang, In situ TEM observation of helium bubble evolution in V/Ag multilayer during annealing, Journal of Nuclear Materials 467, Part 2 (2015) 537-543.

[23] D. Chen, N. Li, D. Yuryev, J.K. Baldwin, Y. Wang, M.J. Demkowicz, Self-organization of helium precipitates into elongated channels within metal nanolayers, Science Advances 3(11) (2017).

[24] M.J. O'Keefe, J.T. Grant, J.S. Solomon, Magnetron sputter deposition of A-15 and bcc crystal structure tungsten thin films, Journal of Electronic Materials 24(8) (1995) 961-967.

[25] T.J. Petty, M.J. Baldwin, M.I. Hasan, R.P. Doerner, J.W. Bradley, Tungsten 'fuzz' growth re-examined: the dependence on ion fluence in non-erosive and erosive helium plasma, Nuclear Fusion 55(9) (2015) 093033.

[26] Y. Noiri, S. Kajita, N. Ohno, Nanostructure growth by helium plasma irradiation to tungsten in sputtering regime, Journal of Nuclear Materials 463 (2015) 285-288.

[27] M.J. Baldwin, R.P. Doerner, Helium induced nanoscopic morphology on tungsten under fusion relevant plasma conditions, Nuclear Fusion 48(3) (2008) 035001.

[28] F. Sefta, K.D. Hammond, N. Juslin, B.D. Wirth, Tungsten surface evolution by helium bubble nucleation, growth and rupture, Nuclear Fusion 53(7) (2013) 073015.

[29] A.M. Ito, A. Takayama, Y. Oda, T. Tamura, R. Kobayashi, T. Hattori, S. Ogata, N. Ohno, S. Kajita, M. Yajima, Y. Noiri, Y. Yoshimoto, S. Saito, S. Takamura, T. Murashima, M. Miyamoto, H. Nakamura, Molecular dynamics and Monte Carlo hybrid simulation for fuzzy tungsten nanostructure formation, Nuclear Fusion 55(7) (2015) 073013.

[30] R.P. Doerner, M.J. Baldwin, M. Simmonds, J.H. Yu, L. Buzi, T. Schwarz-Selinger, Quantitatively measuring the influence of helium in plasma-exposed tungsten, Nuclear Materials and Energy 12 (2017) 372-378.

[31] P. Fiflis, N. Connolly, D.N. Ruzic, Experimental mechanistic investigation of the nanostructuring of tungsten with low energy helium plasmas, Journal of Nuclear Materials 482 (2016) 201-209.

[32] G.Y. Huang, N. Juslin, B.D. Wirth, First-principles study of vacancy, interstitial, noble gas atom interstitial and vacancy clusters in bcc-W, Computational Materials Science 123 (2016) 121-130.

[33] N. Zhang, Y. Zhang, Y. Yang, P. Zhang, Z. Hu, C. Ge, Trapping of helium atom by vacancy in tungsten: a density functional theory study, The European Physical Journal B 90(5) (2017).

[34] S.S. Gupta, M.A. van Huis, M. Dijkstra, M.H.F. Sluiter, Depth dependence of vacancy formation energy at (100), (110), and (111) Al surfaces: A first-principles study, Physical Review B 93(8) (2016) 085432.

[35] L. Sun, S. Jin, G.-H. Lu, L. Wang, High hydrogen retention in the sub-surfaces of tungsten plasma facing materials: A theoretical insight, Scripta Materialia 122 (2016) 14-17.

[36] D. Nguyen-Manh, S.L. Dudarev, Trapping of He clusters by inert-gas impurities in tungsten: First-principles predictions and experimental validation, Nuclear Instruments and Methods in Physics Research Section B: Beam Interactions with Materials and Atoms 352 (2015) 86-91.

[37] J. Wang, Y. Zhang, H.B. Zhou, S. Jin, G.H. Lu, First-principles investigation of helium dissolution and clustering at a tungsten (110) surface, Journal of Nuclear Materials 461 (2015) 230-235.

[38] H.B. Zhou, Y.H. Li, G.H. Lu, Modeling and simulation of helium behavior in tungsten: A first-principles investigation, Computational Materials Science 112 (2016) 487-491.

[39] G.Y. Pan, Y.G. Li, Y.S. Zhang, C.G. Zhang, Z. Zhao, Z. Zeng, First-principles investigation of the orientation influenced He dissolution and diffusion behaviors on W surfaces, RSC Advances 7(41) (2017) 25789-25795.

[40] L. Wang, W. Hu, H. Deng, S. Xiao, J. Yang, F. Gao, H.L. Heinisch, S. Hu, Helium nanobubble release from Pd surface: An atomic simulation, Journal of Materials Research 26(3) (2011) 416-423.

[41] L. Liang, M. Ma, W. Xiang, Y. Wang, Y. Cheng, X. Tan, A molecular dynamics simulation study of temperature and depth effect on helium bubble releasing from Ti surface, Journal of Alloys and Compounds 645 (2015) S166-S169.

[42] B.L. Zhang, J. Wang, M. Li, Q. Hou, A molecular dynamics study of helium bubble formation and gas release near titanium surfaces, Journal of Nuclear Materials 438(1) (2013) 178-182.

[43] E.M. Bringa, J.D. Monk, A. Caro, A. Misra, L. Zepeda-Ruiz, M. Duchaineau, F. Abraham, M. Nastasi, S.T. Picraux, Y.Q. Wang, D. Farkas, Are nanoporous materials radiation resistant?, Nano letters 12(7) (2012) 3351-5.

**Tables**

**Table 1.** The ERD results display relative He concentrations in the irradiated nanochannel W films and bulk samples compared to the reference sample bulk W to the fluence $3\times10^{17}$ ions/cm$^2$.

| **Fluence (ions/cm$^2$)** | **3 ($\times10^{17}$)** | **5 ($\times10^{17}$)** | **10 ($\times10^{17}$)** |
|---|---|---|---|
| W-RT -150W | 2.65 | 3.52 | 3.63 |
| W-600-150W | 2.93 | 4.49 | 5.38 |
| W-600-50W | 2.98 | 4.78 | 4.98 |
| bulk W | 3.00 | 4.54 | 5.23 |

**Figures**

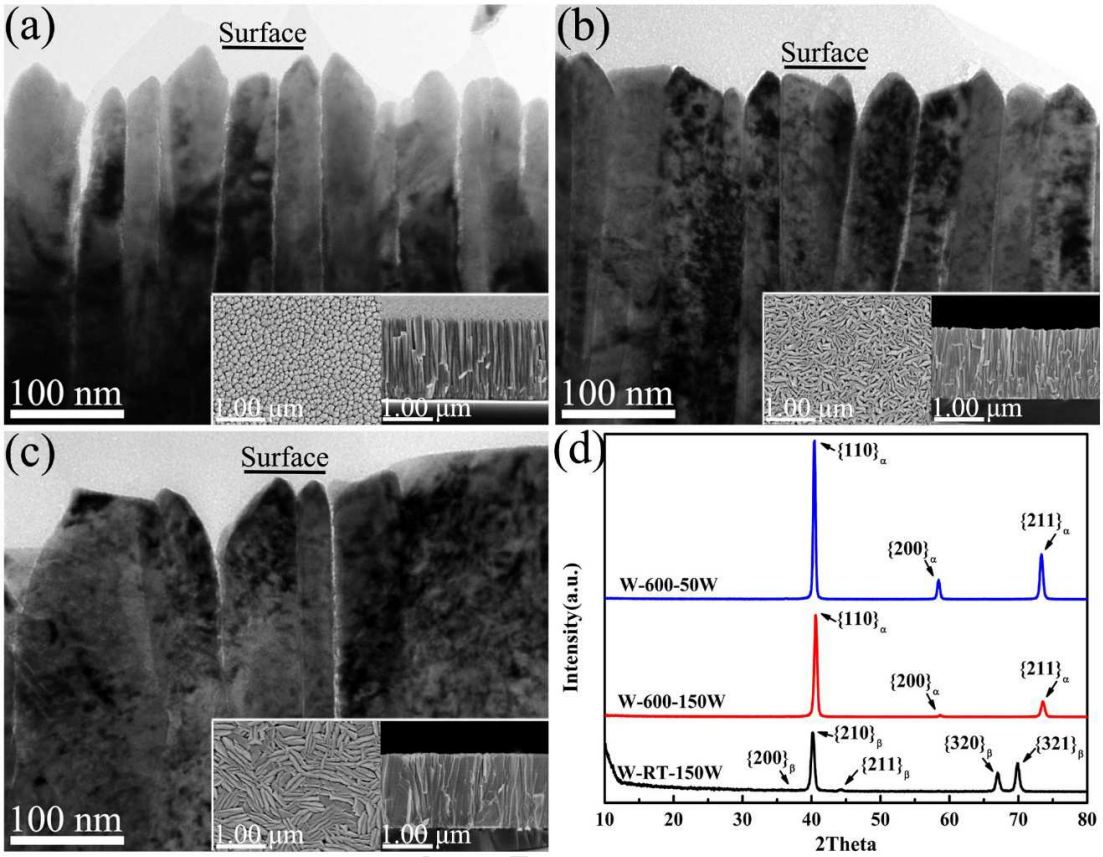


**Fig. 1. XTEM images of as-deposited nanochannel W films.** (a) W-RT-150W, (b) W-600-150W, (c) W-600-50W. Inserts in (a)-(c) are corresponding plan-view and cross-sectional SEM micrographs. (d) is the corresponding GIXRD image.

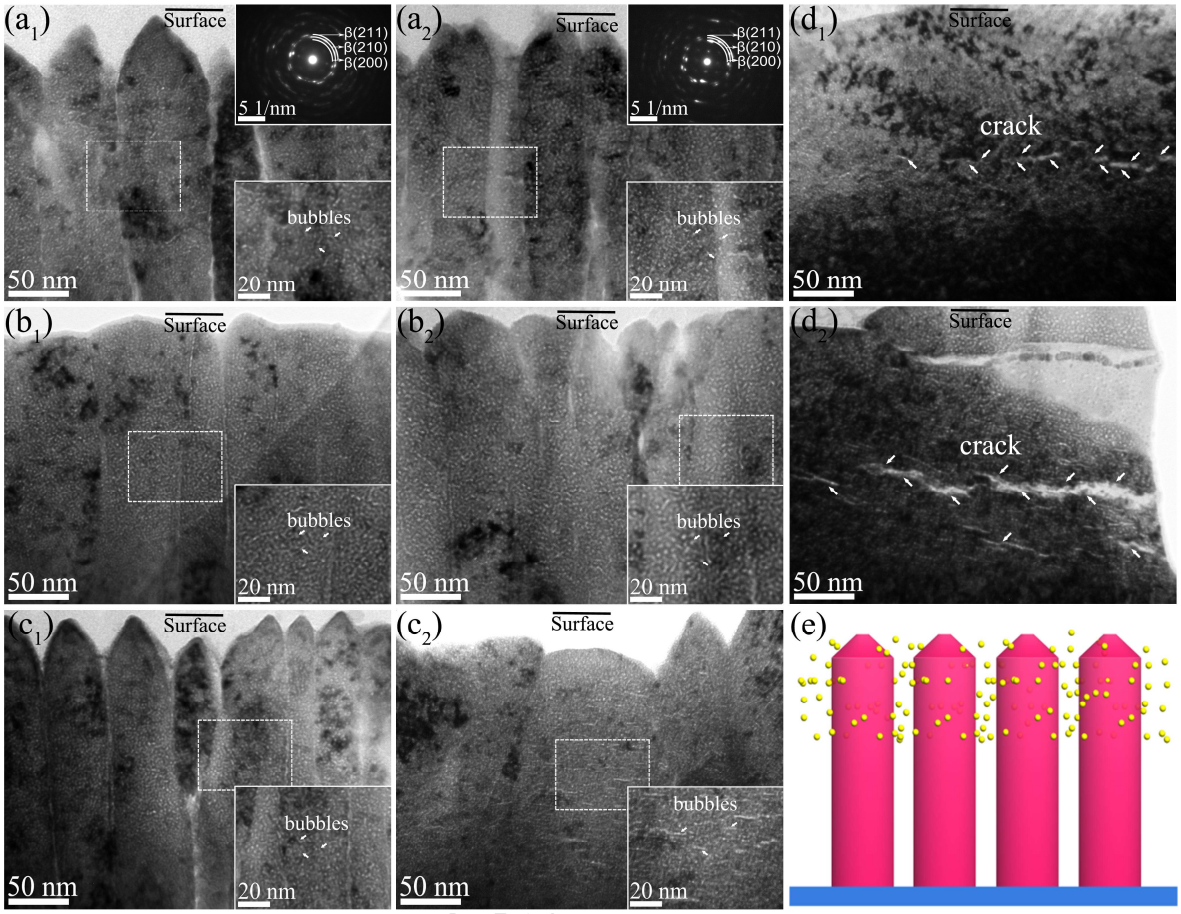


**Fig. 2. XTEM images of the irradiated nanochannel W films and bulk W to the fluence of $5\times10^{17}$ ($a_1$-$d_1$) and $1\times10^{18}$ ions/cm$^2$ ($a_2$-$d_2$).** The nanochannel films ($a_1$-$a_2$) W-RT-150W, ($b_1$-$b_2$) W-600-150W, ($c_1$-$c_2$) W-600-50W and ($d_1$-$d_2$) bulk W. (e) Model of diffusion of He bubbles (yellow ball) in the nanochannel W films (deep pink column). The corresponding magnified images of the regions near 108 nm are marked by dotted line. The SAED pattern of W-RT-150W is inserted in the upper right of image ($a_1$-$a_2$).

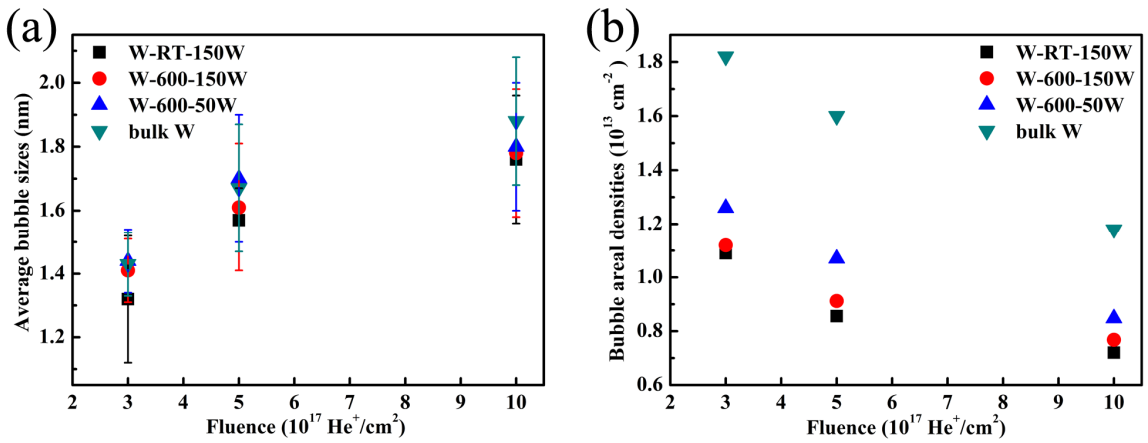


**Fig. 3. Statistical results of the average bubble size and areal densities in the irradiated samples.** Average bubble sizes (a) and bubble areal densities (b) of nanochannel films W-RT-150W, W-600-150W, W-600-50W and bulk W as a function of fluence.

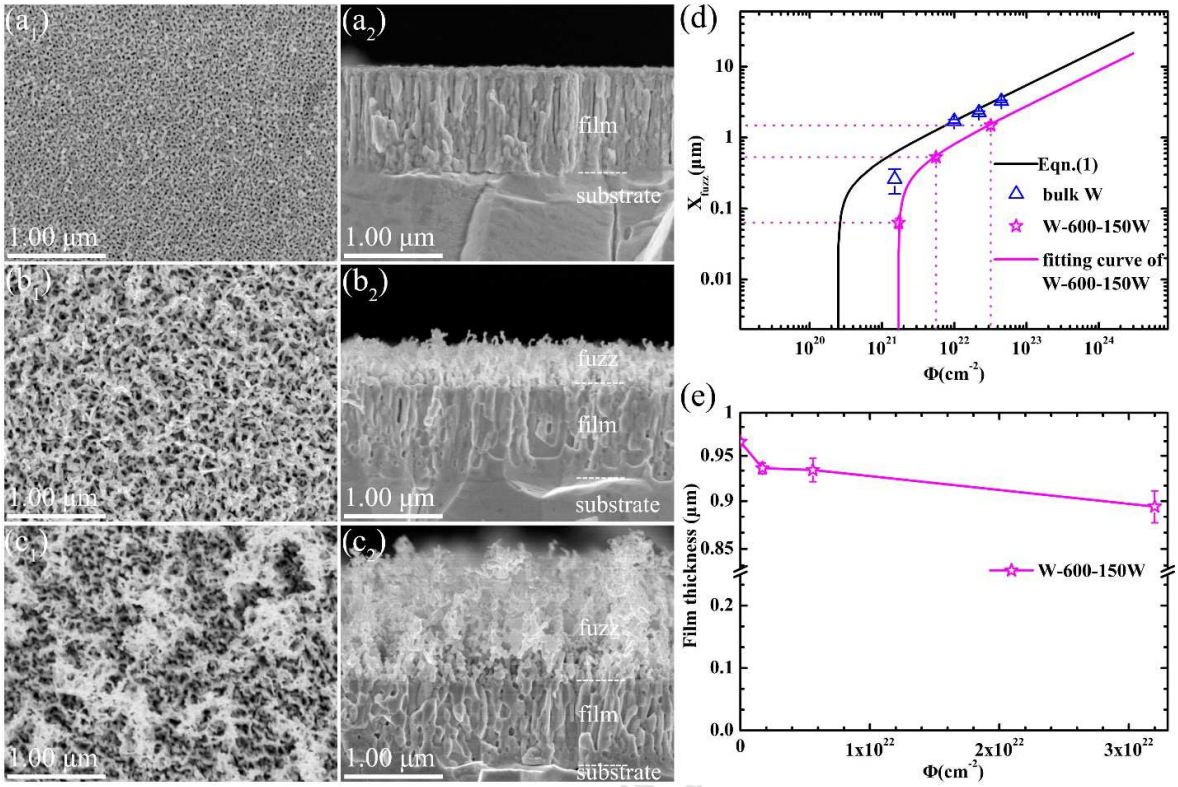


**Fig. 4. SEM images ($a_1$-$c_1$) and corresponding cross-sectional SEM images ($a_2$-$c_2$) of the nanochannel W-600-150W films exposed to the pure He plasma at 1140K and relevant curves.** The fluences are $1.7\times10^{21}$ ions/cm$^2$ ($a_1$) ($a_2$), $5.6\times10^{21}$ ions/cm$^2$ ($b_1$) ($b_2$), $3.2\times10^{22}$ ions/cm$^2$ ($c_1$) ($c_2$), respectively. The "fuzz" thickness against $He^+$ ion fluence is plotted (black line) according to Equation (1) and shown in (d). "Fuzz" thickness of the nanochannel W-600-150W film measured from ($a_2$-$c_2$) and corresponding fitting curve for the nanochannel film (magenta line), and the reference bulk W are also described in (d). Film thickness of nanochannel W-600-150W film before and after irradiation are plotted in (e).

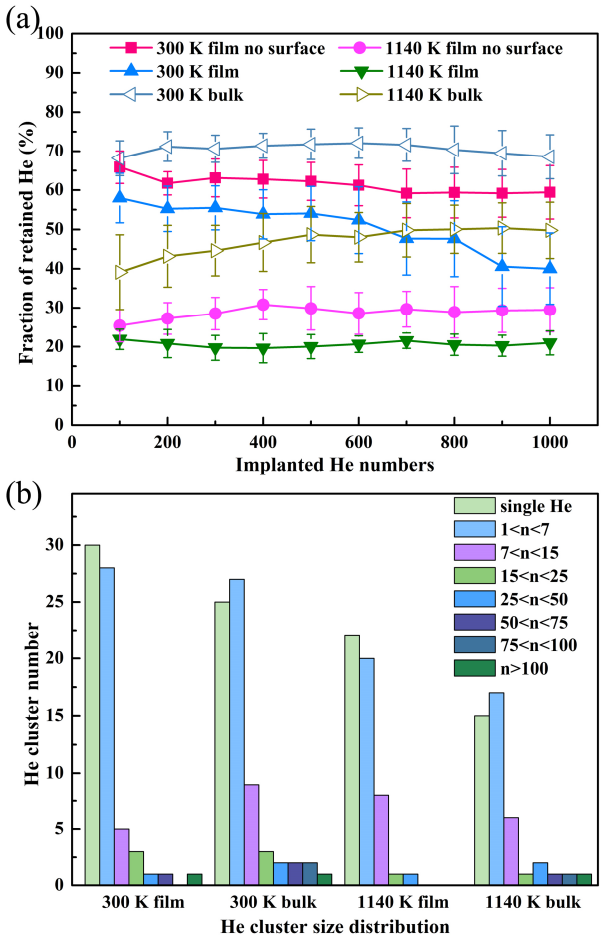


**Fig. 5. The simulation results of $He^+$ ions irradiated to the nanochannel W film and bulk W.** (a) Fraction of He retained in the nanochannel W film and the film without (100) surface at 300 and 1000 K, respectively, the fraction of He retained in the bulk W value (hollow shaped line) is also depicted as a reference. (b) The He cluster size distributions in the nanochannel W film and bulk W at different temperature are plotted.

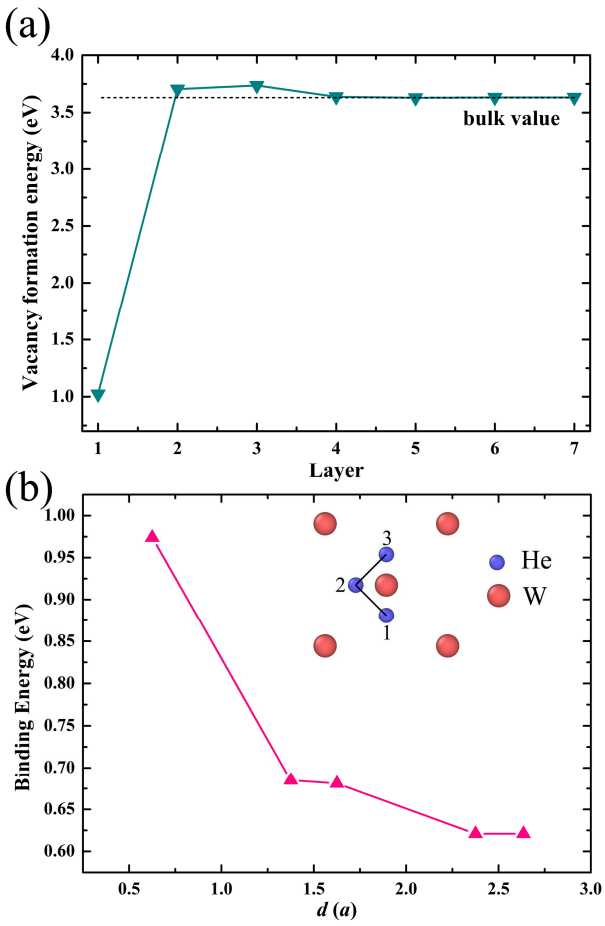


**Fig. 6. Simulation results of vacancy formation and He atoms binding energy.** (a) Variation of vacancy formation energy with different layers from surface. (b) He-He binding energy as a function of different depths (*d*) from the surface, in which *a* is the lattice constant. Insect is a unit cell of W (red ball) with three TIS He (blue ball) atoms, where 1 and 2, 2 and 3 are the first nearest neighbor, 1 and 3 are the second nearest neighbor.